F. Vignati, A. Guardone
Multi-Domain Simulations of Shock Wave Interaction with Aerodynamic Obstacles in Cylindrical Implosions
Journal of Computational and Applied Mathematics, Vol. 283, 2015, p. 218-227
doi:10.1016/j.cam.2014.12.039

Multi-domain Simulations of Shock Wave Interaction with Aerodynamic Obstacles in Cylindrical Implosions

F. Vignati, A. Guardone *

Department of Aerospace Science and Technology, Politecnico di Milano
Via La Masa, 34 - 20156 Milano, Italy

Abstract

A multi-domain finite-volume approach is presented to simulate the interaction of converging shock waves and aerodynamic obstacles for dilute gases. The so-called reshaping process, in which the cylindrical shock is reshaped into a polygonal shock due to the presence of obstacles along the shock path, in studied. To accurately capture the diverse spatial scales of the problem, the computational domain is divided into three sub-domains, namely, the far-field region, the obstacle region and the focus region. Shock propagation in the far-field region is simulated under the axisymmetric, namely, one-dimensional approximation. The obstacle region is described by a fully two-dimensional model, in which initial conditions are interpolated from the far-field. The solution in the obstacle region is then interpolated into the focus region surrounding the center of the imploding shock. These two regions partially overlap to allow for linear interpolation. Numerical results are presented for air in dilute conditions and for four, eight, sixteen and twenty four aerodynamic obstacles. The proposed multi-domain solution technique is found to be capable of describing the complex gasdynamics of the shock propagation and reshaping, while reducing the computational burden for a large number of obstacles of one order of magnitude with respect to fully two-dimensional simulations.

Key words: Finite volume solver, Multi-domain approach, Converging shock waves, Aerodynamic obstacles, Shock reshaping, Ideal gas

* Corresponding author
Email addresses: federica.vignati@mail.polimi.it (F. Vignati), alberto.guardone@polimi.it (A. Guardone).

1 Introduction

The knowledge about converging shock waves is relevant to both theoretical gasdynamics—in e.g. the study of the instability of the shock front and of sonoluminesce— and to industrial applications, including Inertial Confinement Fusion (ICF) [1]. In ICF applications, large values of the temperature and pressure are required to trigger thermonuclear reactions and are expected to be observed in the close proximity of the shock focus point. Unfortunately, to attain high energy concentration at the focus point, it is mandatory to cope with the intrinsic instability of imploding cylindrical shock waves. Shock front instability may be triggered in certain thermodynamic [2] or flow [3] conditions. The main consequence of the deviation of the shock shape from regularity is a reduction of its effectiveness in terms of the maximum values of the pressure and temperature at the focus point.

To prevent the onset of shock instabilities, one can force the shock to interact with a number of obstacles placed along its propagation path. The multiple reflections of the shock eventually modify its shape into a more stable one. For symmetrically arranged and suitably shaped obstacles , the final shock shape is prismatic, which corresponds to a more stable configuration [6,10]. On the other hand, the obstacle arrangement is to be optimized to reduce losses due to shock/obstacle interaction [4]. Numerical simulations were used to determine the optimal design of the obstacle shape and arrangements. In particular, aerodynamic obstacles were proposed to reduce shock/obstacle interaction losses [5]. Due to the diverse time and space scales involved, the numerical simulations of the reshaping process and shock focusing is not trivial.

In the present work, a multi-domain approach is proposed to reduce the computational effort required by shock reshaping simulations while preserving an overall accuracy that is sufficient to capture the relevant flow features, including the temperature peak at the focus point. Differently from reference [6], where the complete configuration is simulated, the diverse symmetries of the problem are exploited here in order to reduce the size of the computational domain: a one-dimensional axisymmetrical simulation is performed far from the obstacle region where the implosion can be represented by a shock wave with cylindrical symmetry. Then, two concentric two-dimensional numerical domains are used to represent respectively the reshaping phenomenon, which is the core of the investigation, and the focusing of the shock at the origin. Each simulation is initialized with the results of the previous one. To this purpose, a 1D/2D and a 2D/2D interpolation procedure is devised and implemented in the FlowMesh software of the Department of Aerospace Science and Technology of Politecnico di Milano [7,8]. In the FlowMesh solver, the fluid-dynamic governing equations are solved in the Arbitrary Eulerian-Lagrangian

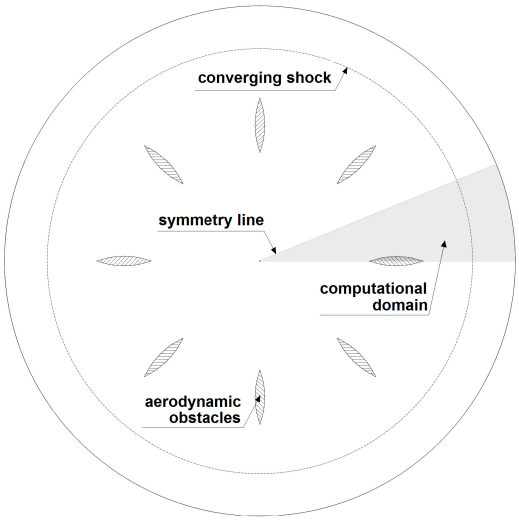

Fig. 1. Sketch of the problem geometry. The shaded region is the computational domain correspinding to the obstacle region

formulation, based upon a Finite Volumes space discretization.

This paper consists of three sections: the first one presents an overview of the physical problem and of its most relevant features. The second section illustrates the procedure adopted in the setup of the numerical simulations, with particular reference to the decomposition of the problem and the interface-matching technique. The third section presents numerical results obtained by applying the different strategies to the simulation of the reshaping of cylindrical shocks. In the last section, final remarks and future development of the present work are presented.

2 Physics of the interaction process

The present section briefly outlines the relevant features of the physical problem of interest. The obstacle arrangement and an overview of the considered problem geometry is depicted in Figure 1, where the three-dimensional cylindrical shock front is represented in a two-dimensional plane that is normal to the symmetry axis. In Figure 1, the dashed line indicates the shock position before interacting with the obstacle leading edges. As it moves towards the origin, the shock interacts with the aerodynamic obstacles which are placed around the origin in a symmetric fashion. The final goal is to reshape the curved shock wave into a polygonal shock, whose piece-wise straight front is more stable with respect to surface corrugations [9]. According to previous investigations [10], the best results are obtained for symmetrical obstacle arrangements. In this case, the number of edges of the final configuration is

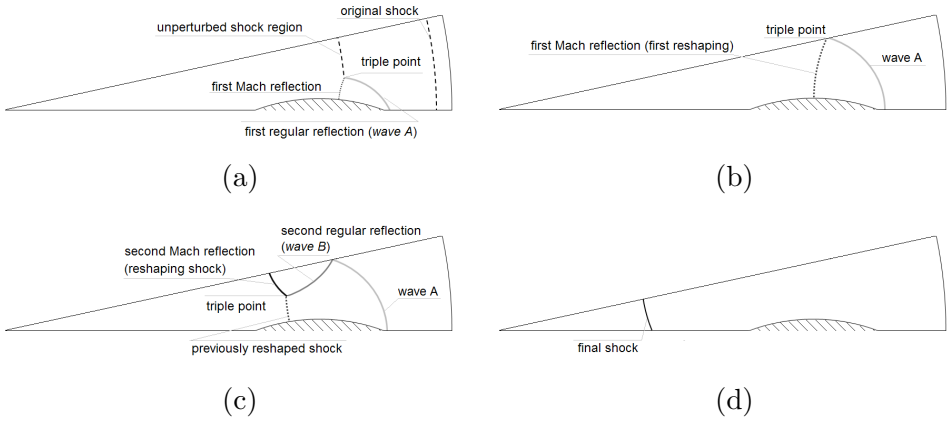

Fig. 2. Sketch of the series of reflections causing the shock reshaping.

equal to the number of obstacles (or twice as many) and the vertices of the polygonal shock are located along symmetry lines, namely, along the obstacle axes or the median lines separating each couple of obstacles.

Thanks to the symmetric arrangement of the obstacles, the shock dynamics can be conveniently described in a reduced domain, labeled sub-domain in Figure 1, which spans an angular sector of π/n_{obs} — where n_{obs} is the number of obstacles.

In Figure 2, the reflection patterns causing the shock reshaping are sketched. The first reflection occurs at the obstacle leading edge (Fig. 2(a)) and for the investigated obstacle geometry it is known to be of Mach type, characterized by the presence of a triple point, moving towards the median symmetry line, where the incident shock front and the two reflected waves (the Mach stem and the simple reflection, namely wave A) intersect. The second step is the reflection at the symmetry surface (Fig. 2(b)), which produces a second Mach reflection followed by a second simple reflection, identified as wave B (Fig. 2(c)). These two shocks intersect the first Mach stem (indicated as previously reshaped shock in the figure) at the second triple point. At this stage, the reshaping process resulted in a polygonal shock consisting of $2n_{\mathrm{obs}}$ edges, whose relative lengths are time-dependent. Finally, as the second triple point reaches either the obstacle or the horizontal boundary, the shock consists of a polygonal front with n_{obs} edges (Fig. 2(d)): the reshaping may now be considered concluded, but the combination of geometrical and fluid-dynamic factors may possibly results in further Mach reflections, at the symmetry lines downstream the obstacles or on the obstacle itself. In the latter case, the polygonal shock undergoes a continuous reshaping, which results in a similar shock front, with vertices located along symmetry lines [11].

To conclude, it is to be noted that the final shock front is not perfectly polygonal, because of the concavity of the shock sides, which are usually curved outwards. However, the edges curvature is usually very small, and therefore

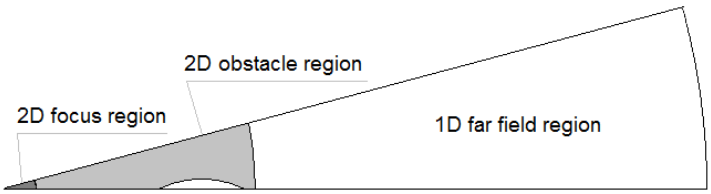

Fig. 3. Sketch of the subdivision into three of the subdomain: from right to left, the *far field region*, the *obstacle region* and the *focus region*.

these shock waves are usually referred to as "polygonal" shocks.

3 Multidomain computational procedure

This section outlines the multi-domain approach proposed in this work. With reference to Figure 3, it is possible to define three different steps separated in both space and time during the reshaping process. The hyperbolic nature of the problem allows us to split the computational domain into three regions, respectively upstream, in proximity and far downstream the obstacle, as depicted in Figure 3.

Upstream the obstacle, the cylindrical shock is originated and propagates inwards. The one-dimensional axisymmetrical simulation of the shock propagation in this zone, namely the *far field region*, is described in section 3.1. The two-dimensional shock/obstacle interaction and the resulting reshaping are detailed in section 3.2, which describes the reflections taking place in the *obstacle region*. Finally, the polygonal shock focusing is simulated on a two dimensional computational domain which includes the origin, that is the *focus region*: the latter simulation and the interpolation technique which allows the initialization of this calculation are illustrated in section 3.3

3.1 Far field region

By assuming that the shock is initially stable, an axisymmetric model can be used up to the obstacle leading edges. The shock propagation before the reshaping can therefore be determined by means of one-dimensional axisymmetrical calculation, initialized with a circular pressure and density step imposed on still gas [12,13]. Such an initial condition results in the formation of the envisaged converging shock as well as a contact discontinuity moving towards the focus point and an outwards propagating rarefaction wave. Besides the flow variation across these waves, unlike the planar shock propagation, the radial distribution of the flow quantities is not uniform and must be deter-

mined numerically. Although the region upstream the obstacle is not involved in the reshaping process, the initial pressure step must be imposed far enough from the leading edges to allow for the shock front to reshape and reach the origin before the contact discontinuity interacts with the obstacles. Preliminary simulations allowed us to observe that, in the explored range of pressure and density, the minimum distance between the pressure step and the center corresponds to five times the chord of the obstacles: this means that the size of the computational domain is much larger than the simple region where the reshaping and the focusing take place, and that a very large computational time would be required for the full two-dimensional simulation of the formation and propagation of the waves upstream the obstacles which are of no interest in this work.

The detection of the shock position, and therefore of the ending of the simulation, is performed by means of a modified Payne method, as detailed in section 3.2.

3.2 Obstacle region

The reshaping process is investigated by means of a fully two-dimensional simulation performed on the sub-domain in Figure 1. The multi-domain approach allows us to exclude from the computational domain the tail of the distribution of density, momentum and total energy far upstream the obstacles, that include phenomena of no relevance such as the contact discontinuity and the rarefaction wave and, consequently, to reduce the number of nodes and the required time. This is accomplished by initializing the two-dimensional calculations with the interpolation on the obstacle region mesh of the solution of the previous one-dimensional axisymmetrical simulation. Boundary conditions of the external boundary are of non-reflecting type.

In order to capture the complete reshaping process, it is necessary to include in this region not only the portion strictly surrounding the obstacle, but also a significant zone downstream. Nevertheless, the focus region is to be excluded, in order to avoid the presence of elements with an excessive aspect ratio in correspondence of the vertex of the slice, especially in cases with several obstacles, where the elements in the origin would be extremely stretched. Indeed triangular elements at the origin are associated to a minimum angle of $\pi/2n_{\mathrm{obs}}$. It is verified within this work that, especially from twenty four obstacles up, calculations suffer from a lack of accuracy in correspondence of the origin, due to the poor quality of the elements. As a consequence, the effective computational domain is the one previously indicated as subdomain, excluding the region very close to the focus point.

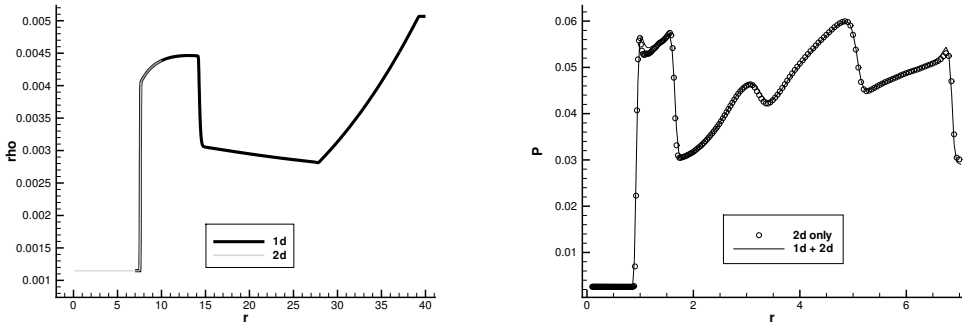

(a) (b)

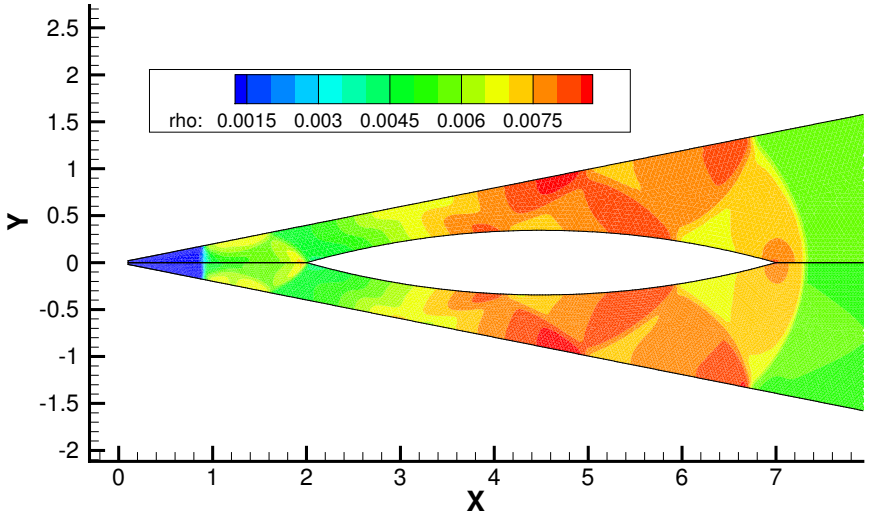

(c)

Fig. 4. Results of the simulations of the propagation of a shock generated by an initial discontinuity located at a radius of 25 unit lengths, with a pressure ratio of 16 (a) Density profiles in the area of overlapping between the one-dimensional simulation (black) and a radial section of the initialized 2D simulation (gray) at the beginning of the simulation of the obstacle region. Correspondence of the pressure profiles on the upper symmetry boundary (b) and the density contours in the domain (c) between a full two-dimensional and a multi-domain simulations at the end of the computation in the obstacle region.

Figure 4 illustrates the correspondence of the density profiles between the one-dimensional solution and a radial section of the two-dimensional case in the overlapping zone. The interpolation between the far field region and the obstacle region is indeed a simple task, due to the fact that the source one-dimensional and ordered grid is uniform: the relative position of old and new nodes is immediately calculated by comparing their radial coordinates only. The advantage offered by this interpolation is two-fold: on one hand the simulation of each single problem is faster with respect to a fully two dimensional simulation; on the other hand, each one-dimensional simulation can be used

for the initialization of several two-dimensional simulations, which share the same initial conditions and differ from each other only because of the obstacles geometrical parameters.

The two-dimensional calculation is stopped before the reshaped shock reaches the inner boundary, corresponding to a circular arc of radius $r_{\min}$ where no-reflection conditions are imposed. The shock position is determined by means of a modified version of the Payne method [14]. In a one-dimensional framework, Payne suggests to compute the shock position r_s from

$$P(r_s, t_n) = \frac{P_b(t_n) + P_{\mathrm{f}}(t_n)}{2} \tag{1}$$

where $P_b(t_n)$ and $P_{\mathrm{f}}(t_n)$ are respectively the pressure values behind and in front of the shock at each time t_n; for converging shocks, Payne identifies P_b with the local maximum in the pressure distribution and P_{f} with $P(0, \forall t_n)$. In the present work, two modifications are introduced to deal with non axisymmetric waves and with a non monotone post-shock pressure profile:

- The shock is assumed to reach a given probe location at time $\overline{t_n}$ provided that
$$\overline{t_n} = t_n \left| \begin{array}{l} \Big\{ [P(t_{n-1}) < P(t_n)] \\ \qquad \& \ [(P(t_{n+1}) - P(t_n)) < (P(t_n) - P(t_{n-1}))] \Big\} \end{array} \right. \tag{2}$$
The above choice was made since the maximum value of the pressure (or of other relevant quantities) may be located not immediately behind the shock but elsewhere in the tail, even in correspondence of the contact discontinuity [15].
- After the reflection over the obstacle, the shock is no longer axisymmetric, and therefore all quantities, including the shock position have a two-dimensional distribution. This difficulty can be circumvented by placing a ring of probes at a fixed radius $r_{\mathrm{probes}} = r_{\min} + \varepsilon$, with ε a threshold chosen a priori as the minimum distance from the internal boundary which guarantees that the shock is still completely inside the computational domain. At each time step, all probes are monitored, and the simulation is stopped as soon as condition (2) is fulfilled at any probe location.

3.3 Focus region

The third region is the so-called focus region surrounding the origin, where the polygonal shock is expected to converge to a single focus point. The angular size of the computational domain related to this third simulation is not of π/n_{obs}, as in the obstacle region, but an integer multiple of it, in order to avoid overstretched elements at the origin. If on one hand this results in a

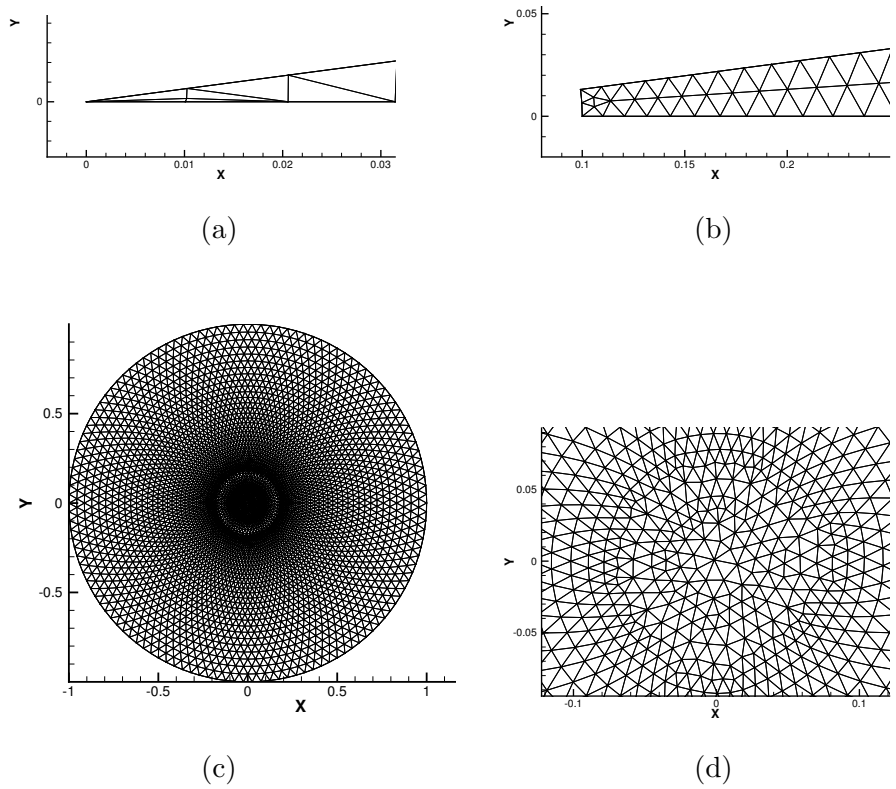

Fig. 5. (a) Zoom of stretched elements in correspondence of the vertex of the full subdomain. (b) Zoom of the higher quality mesh in correspondence of the vertex of the cut subdomain. (c) Focus region mesh (2π case) and close-up in correspondence of the focus point (d).

computational domain larger than theoretically necessary, on the other hand numerical errors due to the overstretched elements can lead to a significant reduction of the accuracy or even prevent to obtain meaningful results.

The simulation over this domain is initialized by means of a linear interpolation of the solution coming from the obstacle region. Albeit the additional error introduced by the interpolation, it is observed that—at the same time step—the solution obtained by applying a multi-domain approach is better than the one obtained from a global domain, because of the numerical errors introduced by the poor quality grid.

Figure 5 illustrates the comparison between the two sub-domains, and the local improvement in the quality of the mesh in correspondence of the origin in the multi-domain case. It is observable that even though the vertex cutoff does not affect the grid on a macroscopic scale (see, e.g, figure 4(c)), the difference becomes relevant close to the origin (pictures 5(a) and 5(b)).

Figure 6 illustrates a flowchart which summarizes the symmetry-exploiting interpolation from the obstacle onto the focus region.

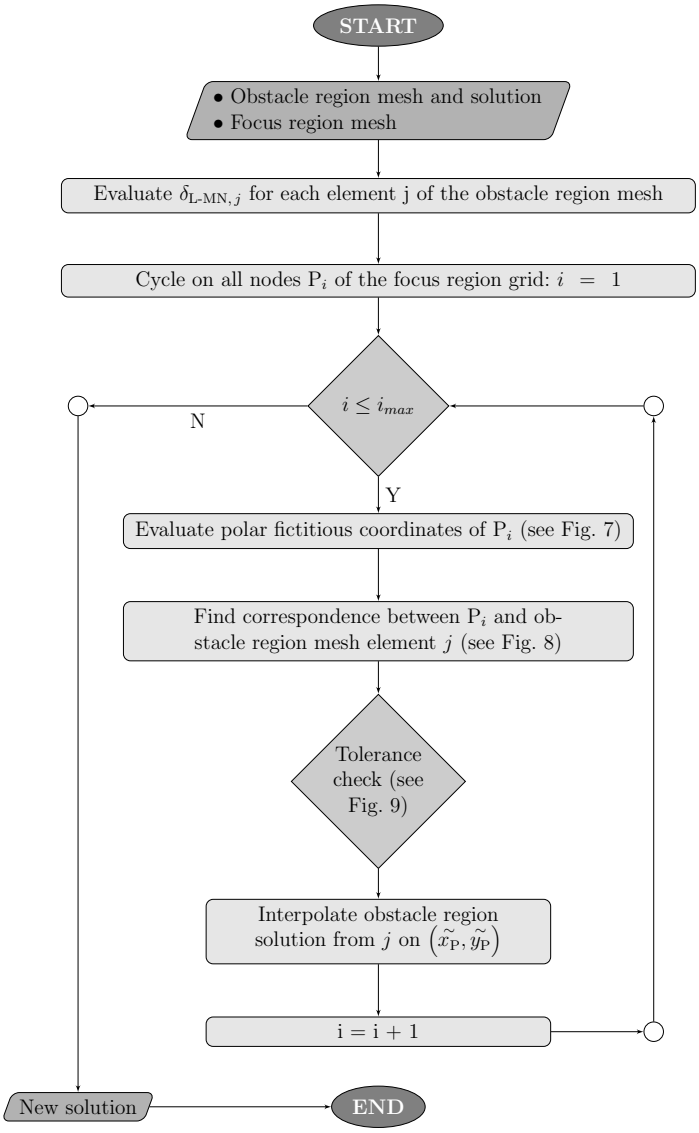

Fig. 6. Flowchart of the algorithm for the interpolation from the solution obtained in the reshaping region to the grid to be used to explore the focusing.

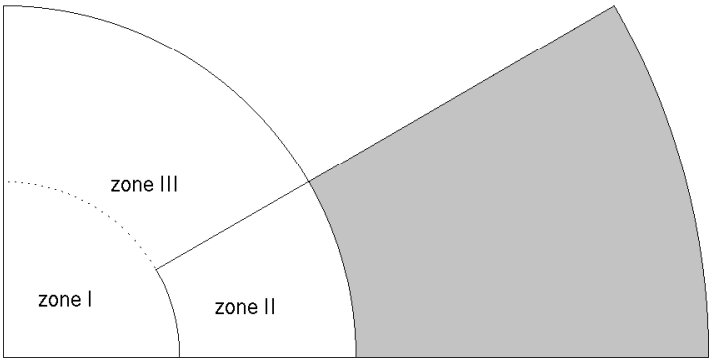

Fig. 7. Subdivision of the focus region domain into three areas, requiring different treatments (proportions exagerated for clarity purposes).

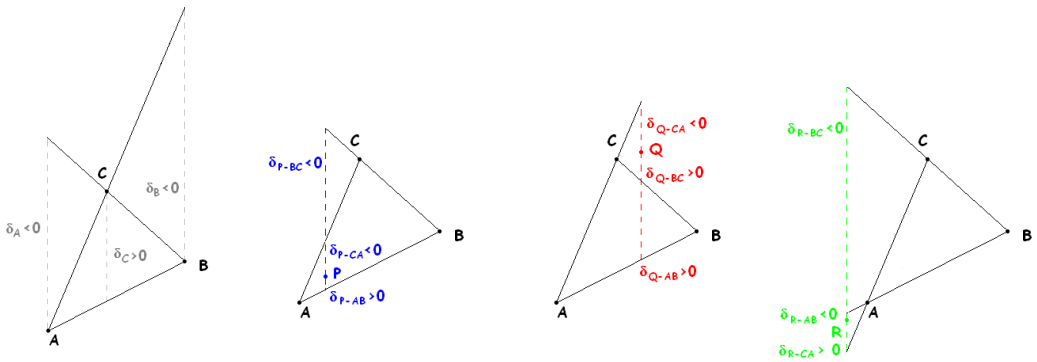

(a) (b) (c) (d)

Fig. 8. Definition of the parameters $\delta\cdot$, j of the element vertices ((a)) and of other points ((b) - (d)). The case reported in (b) is related to the match between the old element j and the node; vice versa (c) and (d) illustrate the case of no correspondence.

With reference to Figure 7, if the generic node P of the focus region grid belongs to zone I, no interpolation is required and the unperturbed solution is imposed. Otherwise, if P belongs to zone II, the element j of the obstacle region mesh including node P is identified and and the interpolation is performed over element j. If instead P belongs to zone III, a fictitious polar coordinate is computed to identify the symmetric point $\widetilde{\mathrm{P}}$ in region II, where interpolation can be carried out.

The parental element of a given node P is that for which

$$\beta_{\mathrm{BC},j} = \delta_{\widetilde{\mathrm{P}-\mathrm{BC},j}} \cdot \delta_{\mathrm{A\text{-}BC},j} \geq 0 \tag{3}$$

for any permutation of the element vertices B, C and A, see Figure 8.

Particular care is to be taken for boundary nodes if the domain boundaries are

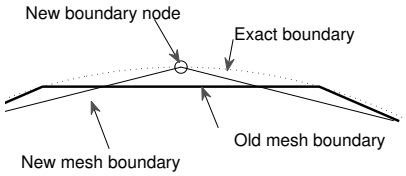

Fig. 9. Example of missing correspondence between a new boundary node (∘) and the old grid due to the boundary discretization (dimensions exagerated for clarity).

curved, as illustrated in figure 9. In these cases, the above inclusion criteria is relaxed to $\beta_{\mathrm{MN},j} \geq \epsilon$, where $\epsilon < 0$ is a tolerance. The initial value of ϵ is very close to zero, and iteratively amplified until either a correspondence is found or ϵ reaches a maximum value. This occurrence has never manifested in any of the actual test cases, where the adopted meshes were fine enough to bound the error introduced by the spatial discretization within the maximum tolerance.

4 Numerical results

Numerical results are presented in this section, to assess the effectiveness of the multi-domain approach. All reported results are related to shocks generated by an initial pressure and density step located at a non-dimensional radius $r_{\mathrm{step}} = 25$. Results are reported for initial external/internal pressure ratio $p_{\mathrm{ext}}/p_{\mathrm{int}} = 16$, but ratios up to 32 are considered to investigate the robustness and accuracy of the procedure.

First, a comparison between the computational times required by the simulations of the shock formation and reshaping in the cases of eight and sixteen obstacles is shown in Table 1. All four cases were simulated on triangular grids with a non-dimensional edge size $\Delta x = 0.05$. The computational times are scaled using the time required for the simulation of the obstacle region only (bold cell in Table 1) for eight obstacle case. The time required by the interpolation from the one-dimensional to the two-dimensional domain is not explicitly reported because it is three/four orders of magnitude smaller, regardless of Δx. Calculations were performed on a single core of a six-core Xeon 2.66 GHz CPU, with 2 GB RAM.

As reported in Figure 4, the differences between the solutions calculated by means of a coupled one-dimensional/two-dimensional approach and the one deriving from a two-dimensional calculation only are negligible.

Figure 10 shows the simulation of the reshaping of a shock in a four-obstacle configuration: in this case the high angle of the domain in correspondence of the focus point ($\pi/2$) allows to obtain regular elements everywhere. Therefore,

Table 1
Computational time for to the simulation of the shock in the far field and in the reshaping region. CPU time are scaled with the a reference time of 65 minutes corresponding to the 8-obstacle case simulated on a single core of a six-core Xeon 2.66 GHz CPU, with 2 GB RAM.

Ref. time = 65 min		8 obstacles	16 obstacles
1D + 2D	1D	0.13	
	2D	**1**	**0.58**
	total	1.13	0.71
2d only		28.69	15.89

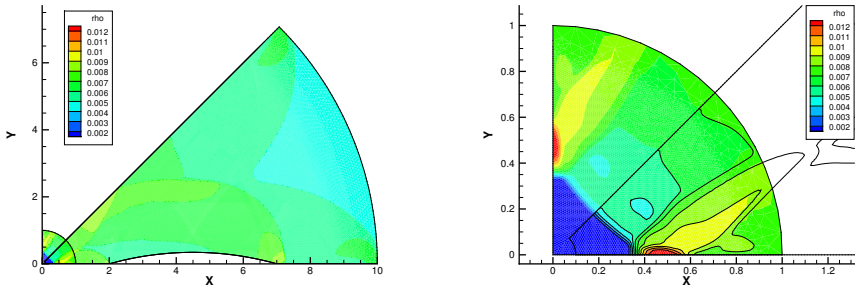

(a) (b)

Fig. 10. Density profiles in the four obstacles case ($\Delta x = 0.01$): (a) coupling between the result of the simulation of the reshaping region and the focus region ($\pi/2$ case) and (b) close-up of the two domains overlapping zone (contours represent the interpolated solutions, isolines the old one).

the results of simulations performed on this domain can be used to explore the correctness of the fit between the two cases, respectively with and without interpolation.

Table 2 provides a comparison among the computational times required for the simulation of the reshaping and focusing depending on the size of the elements; in all the cases reported below the final grid consists of a quarter of circle, with a radius spanning from 0.0 to 1.0:

It can be observed that the additional time introduced by the interpolation is always negligible with respect to the computational time required by the simulation of the shock reshaping. Moreover, even though the focusing is evaluated on a larger domain due to the larger value of the vertex angle—and therefore is computationally more demanding—the simulation of the overall process, that is reshaping and focusing, is globally much faster than the simulation of the same phenomenon on one only domain with larger angles in the origin.

Table 2
Computational times relative to the simulation of the reshaping (obstacle region domain, OR) and the focusing (focus region domain, FR), and to the intermediate interpolation of the solution.

	8 obstacles			16 obstacles		
Δx	OR	interpolation	FR	OR	interpolation	FR
0.015	18.92	0.07	1.32	10.92	0.02	0.92
0.03	7.85	0.02	0.88	3.23	0.01	0.71
0.05	**1**	$4.6{\cdot}10^{-3}$	0.26	0.71	$3.08{\cdot}10^{-3}$	0.18
0.1	0.89	$1.52{\cdot}10^{-3}$	0.05	0.52	$1.03{\cdot}10^{-3}$	0.05

The result of the interpolation from a sixteen obstacles cases (the slice with black edges on the right) to a 2π final computational domain is shown in figure 11(a); the external radius of the focus region domain is exaggerated in order to highlight the quality of the fit between the original and interpolated solutions. The same result is reported in figure 11(b), relative to an eight obstacles case.

The multi-domain approach is applied also to the case of twenty four obstacles. For this number of obstacles the poor quality of the elements in the origin prevents to obtain sufficiently accurate solutions. Therefore, the reference case used for the comparisons is the simulation performed on a domain which includes two obstacles, in order to reduce the aspect ratio of the elements at the origin (namely "doubled domain", see figure 12). The shock position obtained by the multi-domain simulation is compared to that provided respectively by the reference case, a calculation performed on a single domain, see Figure 1),without the multi-domain approach and Guderley self-similar solution [16]:

$$\frac{r(t)}{R_0} = \left(1 - \frac{t}{t_0}\right)^{0.834} \tag{4}$$

The above power-law fit was derived by Guderley for a cylindrical shock; other works provide the power-law exponent also for non-cylindrical shocks, e.g. [6] calculates a value of 0.875 for the eight-sided converging shock. In the twenty four obstacles cases, however, due to the very high number of edges, the shape of the reshaped shock remains close to the circular one, described by Guderley, and therefore the original exponent is adopted.

Figure 13 illustrates a comparison among the analytic solution (full line) and the results of the simulations: it can be observed that the multi-domain approach and the simulation performed on the doubled domain provide very close solutions (the small deviation from Guderley's solution can be attributed to the non perfect circularity of the shock front). On the contrary, closer to the focusing, the simulation on poor quality grid deviates significantly from the reference.

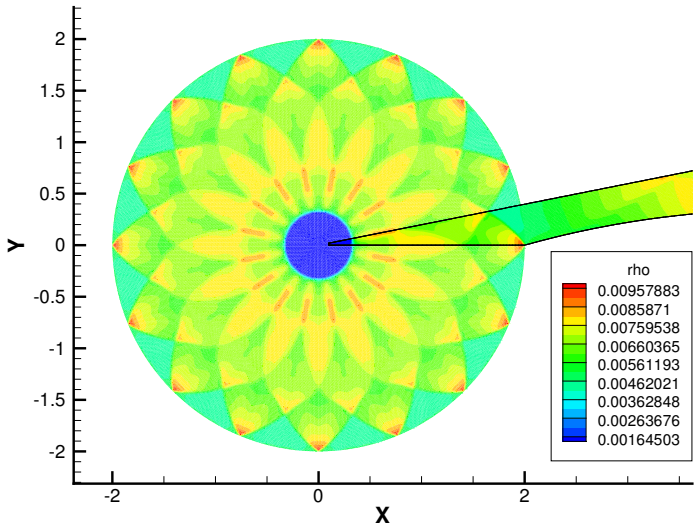

(a)

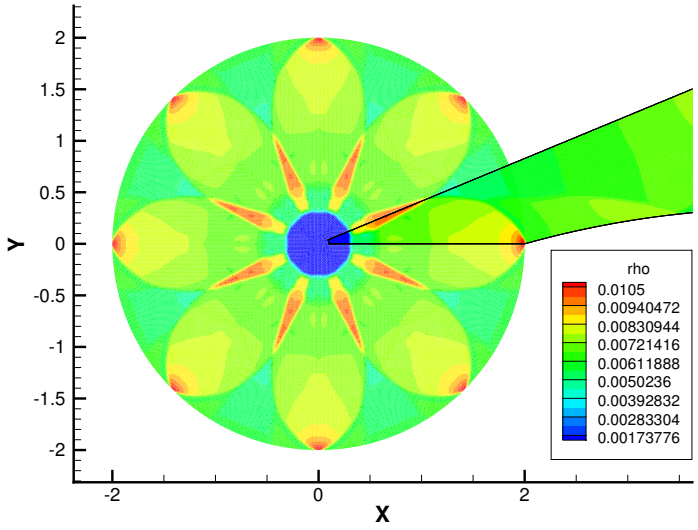

(b)

Fig. 11. Density field in the overlapping zone between the computational domains related to the reshaping region and the focus region, sixteen (a) and eight (b) obstacles cases.

For the same case the compression factors $P_{\max}/P_{\mathrm{f}}$ at the focus point are plotted as functions of time in figure 14. The accordance among the results of the simulations performed on the doubled domain and those obtained by means of the multi-domain approach is very good, whereas the sharp domain underestimates the peak value of the pressure, and poorly captures its trend along

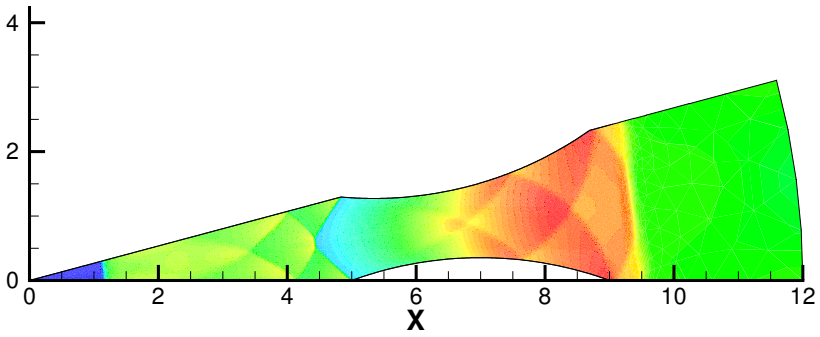

Fig. 12. Simulation of the twenty four obstacles case on a domain including two half obstacles, namely, a doubled domain.

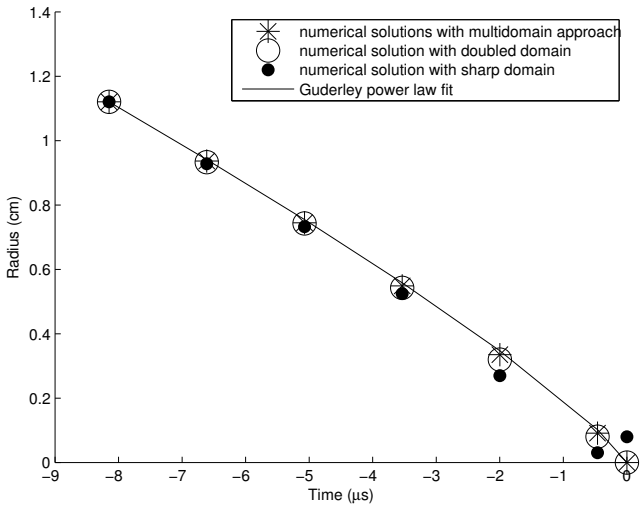

Fig. 13. Shock position as function of time, both referred to the position occupied at an arbitrary time $R_0(t_0) = 1.12048$: comparison between Guderley self-similar solution (full line) and the results of the calculations performed on the doubled domain ($\circ$), with the multi-domain approach ($*$) and on the sharp domain ($\bullet$).

time. The difference in the vertex angle of the computational domain including the focus region ($\pi/2$ and $\pi/12$) does not affect the quality of the solution, provided it is sufficiently large.

5 Conclusions

Numerical experiments on the reshaping of converging shock waves were performed using a novel multi-domain approach. By exploiting to the symmetry of the problem, numerical simulations were performed on a circular sector only. Moreover, the computational domain has then been divided into three parts,

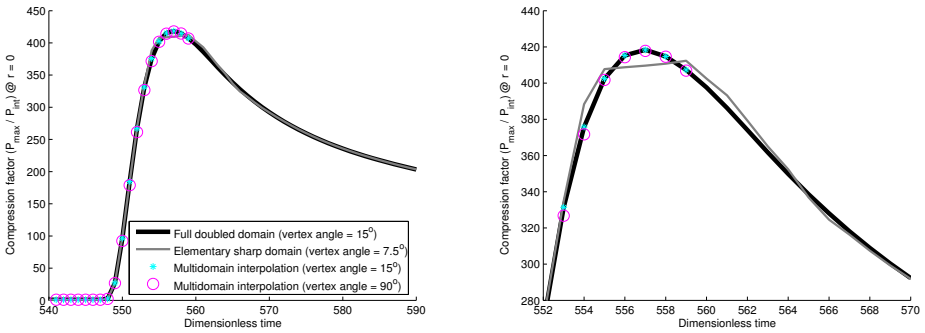

(a) (b)

Fig. 14. (a) Compression factors at the focus point versus time calculated with diverse methods: doubled domain (full black line), multi-domain approach with vertex angle of $\pi/2$ (O), multidomain with vertex angle of $\pi/12$ (∗) and sharp domain (full gray line). (b) Magnification in correspondence of the pressure peak.

the far field region, the obstacle region and the focus region. From the shock formation, taking place in the far field, and until its impingement onto the obstacles, a one-dimensional axisymmetric simulation was performed, whose solution was used to initialize the two-dimensional simulation of the reshaping process. A third region was explicitly introduced to improve the accuracy in the focus region, where the low quality of the elements, resulting from the very sharp angle of the computational domain, introduces significant numerical errors. Therefore, the focusing process was simulated by means of a third calculation performed on a two-dimensional circular sector including the focus point, with an angle large enough to produce a good quality grid, without excessively increasing the number of nodes. A linear interpolation of the solution was used to interface each pair of domains.

A modified version of the Payne method was used in order to detect the arrival of the converging shock and to trigger interpolation from the previous onto the new sub-domain. The modified procedure extends Payne's formulation to the non-axisymmetric case and to implosions in which the pressure peak is not coincident with the shock position.

The symmetry-exploiting multi-domain approach is satisfactory in terms of both computational efficiency and overall accuracy.

The computational time is strongly reduced for several reasons: the reduction of a portion of the two-dimensional domain in a one-dimensional one in the far-field region, the fitness of a single far-field simulation for a wide variety of cases, the possibility of performing symmetry-exploiting two-dimensional simulations even on extremely sharp sub-domains, as opposed to fully circular domain representations. Therefore, it is very fine meshes can be used in all the three regions, due to the less-than-proportional growth in the computational

burden.

The accuracy of the results is preserved also on very stretched domains with high quality meshes by exploiting the intrinsic symmetry of the physical phenomenon. The comparison of the solution with simulations performed on non-subdivided domains and, where possible, self similar law indicates a very good correspondence, along with a strong reduction of the computational time.

References

[1] J.A. Maniscalco *Inertial Confinement Fusion* Annual Review of Energy, 5: 33-60 (1980).

[2] P. Thompson *A fundamental derivative in gas dynamics*, Physics of Fluids 14 (1971) 1843-1849.

[3] R. Perry, A. Kantrowitz *The Production and Stability of Converging Shock Waves*, Journal of Applied Physics 22-7 (1951) 878.

[4] H. Shi, K. Yamamura *The interaction between shock waves and solid spheres arrays in a shock tube*, Acta Mech. Sinica, 20-3 (2004) 219-227.

[5] N. Apazidis, M. Kjellander, N. Tillmark, *High energy concentration by symmetric shock focusing*, Shock Waves 23 (2013), 361-368.

[6] M. Kjellander, N. Tillmark, N. Apazidis, *Thermal radiation from a converging shock implosion*, Physics of Fluids 22 (2010) 046102.

[7] D. Isola, A. Guardone, G. Quaranta, *Arbitrary Lagrangian Eulerian formulation for two-dimensional flows using dynamic meshes with edge-swapping*, Journal of Computational Physics 230 (2011), 7706-7722.

[8] D. Isola, A. Guardone, G. Quaranta, *FlowMesh Solver Website*, www.aero.polimi.it/flowmesh.

[9] V. Eliasson, *On focusing of shock waves*, Ph.D. dissertation, Department of Mechanics, KTH, Sweden (2007).

[10] V. Eliasson, N. Apazidis, N. Tillmark, *Controlling the form of strong converging shocks by means of disturbances*, Shock Waves 17 (2007), 29-42.

[11] V. Eliasson, M. Kjellander, N. Apazidis, *Regular versus Mach reflection for converging polygonal shocks*, Shock Waves 17 (2007) 43-50.

[12] B. Zeldovich Ya., P. Raizer Yu., *Physics of Shock Waves and High-Temperature Hydrodynamic Phenomena*, Academic Press Inc., New York, 1967. Volume 2, Chapter 12.

[13] L. I. Sedov, *Similarity and Dimensional Methods in Mechanics*, Academic Press Inc., New York, 1959. Chapter 4.

[14] R. B. Payne, *A numerical method for a converging cylindrical shock*, Journal of Fluid Mechanics 2-02 (1957), 185-200.

[15] K. P. Stanyukovich, *Unsteady motion of Continuous Media*, Gostekhizdat, Moscow, 1955.

[16] G. Guderley, *Starke kugelige und zylindrische Verdichtungsste in der Nhe des Kugelmittelpunktes bzw. der Zylinderachse*, Luftfahrtforschung 19 (1942), 302-312